Trigonal NHC bis-pyridyl silver(i) complexes: a beacon of light in the darkness of light-emitting electrochemical cells?

Ginevra Giobbio, Lucie Greffier, Sophia Lipinski, Anaïs Montrieul, Jean-François Lohier, Mathieu Linares, Rubén D Costa, Sylvain Gaillard

ARTICLE

Trigonal NHC bis-pyridyl silver(I) complexes a beacon of light in the darkness of light-emitting electrochemical cells?

Received 00th January 20xx,
Accepted 00th January 20xx

DOI: 10.1039/x0xx00000x

Ginevra Giobbio,[a,b] Lucie Greffier,[c] Sophia Lipinski,[b] Anaïs Montrieul,[a] Jean-François Lohier,[d] Mathieu Linares,[e] Rubén D. Costa*,[b] and Sylvain Gaillard*,[a]

Complex [Ag(IPr)($^{3\text{-Me}}$dpa)][PF_6] (**1**) possessing the same combination of ligands than a previously reported [Cu(IPr)($^{3\text{-Me}}$dpa)][PF_6] (**2**) applied in blue-emitting Light-emitting Electrochemical Cells (LEC) has been synthesized and fully structurally and photophysically characterized both, in powder and thin-film. In detail, temperature-dependent steady-state, time-resolved emission experiments, and computational calculations have been performed to understand the impact of nature of the ion metal center on the photophysical and electroluminescent properties. Here, a direct comparison between complexes reveals *i*) a distinct emission behavior such as fluorescence (**1**) *vs*. thermally activated delay fluorescence (**2**) caused by the changes of the nature of the emitting excited states from ligand centered (**1**) to metal-to-ligand charge transfer (**2**), *ii*) an unforeseen crystallinity-dependent emission in **1** that leads to either smooth and non-emissive thin-films or phase aggregated and emissive thin-films, and *iii*) **1**-based LECs with an stable electrical behavior over 100 h that contrasts over the prior-art of a few minutes (**2**).

Introduction

Light-emitting electrochemical cells (LECs) have been now studied for three decades as an alternative or close congener of OLEDs.[1-3] Along the time, many types of emitter have been explored, such as conjugated polymers, ionic transition metal complexes (iTMCs), small molecules, and quantum dots.[4-8] Among the iTMCs, first phosphorescent iridium(III) complexes have been extensively studied as phosphorescent emitters that could allow a theoretically 100 % external quantum efficiency (EQE). Even if really impressive performing LECs have been achieved with iridium(III) complexes (>5000 h stability and external quantum efficiencies of > 20 %), [9,10] they presented too many drawbacks for an industrial spreading, such as price and lack of stable blue-emitting derivatives.[3] Then, copper(I) complexes led the race due to (i) the d^{10} configuration, avoiding non-radiative metal-centered (MC) transition, (ii) their emission mechanism, i.e. thermally activated delayed fluorescence (TADF) allowing also a theoretical 100% EQE, and (iii) the abundance of copper in the Earth crust, making them less expensive.[11-16] Nevertheless, the best performance of LECs developed with copper(I) complexes as emitters have only reached the record of 200 h[17] and only recently *on a par* performance with respect to blue LECs based on iridium(III) complexes.[18-20] To provide stable LEC devices incorporating non-expensive iTMC as emitter, silver(I) complexes appeared recently to be a good compromise between iridium(III) and copper(I) complexes. Indeed, emissive silver(I) complexes are characterized by higher stability and ability to design complexes emitting in the high-energy part of the spectrum compared to their Cu(I)-based analogues.[21,22] In detail, the silver(I) complexes are characterized by a highly blue-shifted emission since the 4d orbitals of silver(I) are often lower in energy compared to ligand-centered orbitals. Thus, their emission is usually characterized by ligand-centered transitions (LC), since MLCT excited states are too high in energy to be accessible.[23-26] In spite of this fact, their use as emitters for LECs is still very rare. In short, Moudam *et al.* showed a yellowish electroluminescent response of heteroleptic silver(I) complexes without disclosing device performance.[27] Fresta *et al.* reported yellow-emitting LECs incorporating silver(I) complexes combining XanthPhos (4,5-bis(diphenylphosphino)-9,9-dimethylxanthene) and bipyridine derivatives, elucidating the device degradation of a few seconds *via* the formation of Ag nanoclusters under device operation. The device was optimized with 2-(4-tert-butylphenyl)-5-(4-biphenylyl)-1,3,4-oxadiazole (PBD) as electron transport layer (ETL), increasing the stability up to 80 h with a good luminance (L_{max}) level of 35 cd/m^2.[28] Of note, the copper-based analogue in LECs showed slightly higher luminance (L_{max} = 54 cd/m^2), but starkly lower stability ($t_{1/2}$ = 1.8 min).[29] Finally, Lipinski et al. reported red-emitting LECs using silver(I) complex bearing XanthPhos and biquinoline derivative

[a] Normandy University, ENSICAEN, UNICAEN, CNRS, LCMT, 1400 Caen, France. E-mail: sylvain.gaillard@ensicaen.fr
[b] Technical University of Munich, Campus Straubing for Biotechnology and Sustainability, Chair of Biogenic Functional Materials, Schulgasse 22, 94315.
[c] Division of Theoretical Chemistry and Biology, School of Engineering Sciences in Chemistry, Biotechnology and Health, KTH Royal Institute of Technology, SE-100 44 Stockholm, Sweden.
[d] Normandy University, ENSICAEN, UNICAEN, CNRS, CRISMAT, 14000 Caen, France.
[e] PDC Centre for High Performance Computing, EECS, KTH Royal Institute of Technology, Stockholm, Sweden.
† Footnotes relating to the title and/or authors should appear here.
Supplementary Information available: [details of any supplementary information available should be included here]. See DOI: 10.1039/x0xx00000x

as ligands. In this case, Ag nanocluster were not formed in solution and devices, while the use of 4,4'-bis(N-carbazolyl)-1,1'-biphenyl (CBP) as hole transport layer led to devices with L_{max} of 12 cd/m^2 and a $t_{1/2}$ of 5 h.[30] Likewise, the copper analogue implemented in the same device architecture led to a lifetime of only 25 min.[31] As far as trigonal silver(I) complexes, we recently reported an interesting aggregation induced emission (AIE) occurring with [Ag(IPr)(bpy)][PF_6] (bpy = 2,2'-bipyridine) that could pave the way of a new class of silver(I) emitter in LEC devices.[32] They featured an stable electrical behavior, but a lack of light response since the active layers did not feature and AIE behavior. Under the spotlight of these works, we envisaged to incorporate analogous *N*-heterocyclic carbene (NHC) silver(I) complexes bearing bis-pyridyl derivative in LEC device.[19,33-34] Here, we are reporting the synthesis, the structural, photophysical and theoretical studies of [Ag(IPr)($^{3\text{-Me}}$dpa)][PF_6] (**1**) (IPr = 2,6-diisopropylimidazolylidene and $^{3\text{-Me}}$dpa = 3,3'-dimethyl-2,2'-dipyridylamine) in comparison with the highly efficient blue emitting copper(I) complex (**2**) that we previously reported (Scheme 1).[33] In short, a direct comparison between complexes reveals an emission mechanism change from fluorescence (**1**) *to* thermally activated delay fluorescence (**2**). This is related to the changes of the nature of the emitting excited states from ligand centered (**1**) to metal-to-ligand charge transfer (**2**). In addition, **1** shows an emission dependent to the crystallinity that leads to highly emissive powders and thin-films that are not suitable for thin-film lighting devices, while smooth films are non-emissive. However, **1**-based LECs featured a stable electrical behavior over 100 h that contrasts over the prior-art of a few minutes (**2**). Overall, this work highlights that this family of silver(I) complexes deserves attention toward activating the emission features by increasing the CT character in the emitting excited state.

Results and discussion

Synthesis and structural characterization

The synthesis started by the preparation of the $^{3\text{-Me}}$dpa ligand following a reported Buchwald-Hartwig coupling using 2-amino-3-methylpyridine and 2-bromo-3-methylpyridine.[33,37] Whereas, the neutral complexes [M(IPr)Cl] **3** and **4** (M = Ag for **3** and M = Cu for **4**) were prepared according to the Nolan and Cazin's procedures for the synthesis of Ag(I) and Cu(I) complexes.[36-38]

With these precursors in at hands, the targeted cationic heteroleptic complexes were synthesized following the procedure already reported for the synthesis of [Cu(IPr)($^{3\text{-Me}}$dpa)][PF_6] and applied for the silver(I) congener.[32,33] Albeit this synthetic strategy is pleasantly effective for Cu(I)-based complexes (98 % isolated yield for **2**),[19,33-34] yield and selectivity decreased significantly for **1**. Indeed, **3** was fully converted into **1** with the formation of 4.5 % of the homoleptic [Ag(IPr)$_2$][PF_6] complex as side product. Then, **1** was successfully purified by slow-gas diffusion crystallization but this purification drastically compromised the isolated yield (30%). At first, the coordination of the carbene ligand (IPr) was detected by ^{13}C NMR due to the characteristic two doublet signals attributed to the direct coupling of the carbon nucleus with the two magnetically active isotopes of silver, i.e. ^{107}Ag and ^{109}Ag, having natural abundance of 51 % and 49 %, respectively.[36] Additionally, ^{1}H NMR spectroscopy showed the expected 1:1 ratio between IPr and $^{3\text{-Me}}$dpa for the formation of the heteroleptic complex **1**. Then, the structure of **1** was confirmed by X-ray diffraction analysis. Indeed, needle-like crystals suitable for this analysis were obtained by using slow gas diffusion recrystallization of a concentrated dichloromethane solution of **1** and diethyl ether as light solvent (Figure 1). Relevant bond lengths and angles were reported in Table 1 along with the data previously reported for **2** for comparison purposes.[33]

The size of the metal center (Ag = 1.65 Å *vs*. Cu = 1.54 Å)[36,39] appeared to play a pivotal effect on the overall structure in both complexes. Indeed, the higher radius of the Ag(I) metal center caused an increase of the bond lengths toward the ligands. In detail, the bond length of Ag–C_{IPr} in **1** was significantly longer than in **2** (2.0744(15) *vs*. 1.921(18)) – Table 1. Then, higher bond lengths in **1** were also observed with the nitrogen atoms of the $^{3\text{-Me}}$dpa ligands, 2.2872(14) and 2.0577(18) for **1** and **2,** respectively. These longer bond lengths between the ligands and the metal center in **1** led to a decrease of the previously defined plan angle θ for **2**, with a value of 22.4 °, and found at 18.29 ° for **1** (Figure 1, right).[33] Of note, albeit considerably planer than **2**, no interactions between metal centers or ligands have been detected in the unit cell of **1**, probably due to the steric hindrance generated by the isopropyl groups out of the plane of the metal center. Finally, the presence the methyl groups in 3- position to the pyridine rings do not allow intermolecular π-π interactions which had a key-role in the photophysical behavior of recently reported trigonal silver(I) complexes.[32]

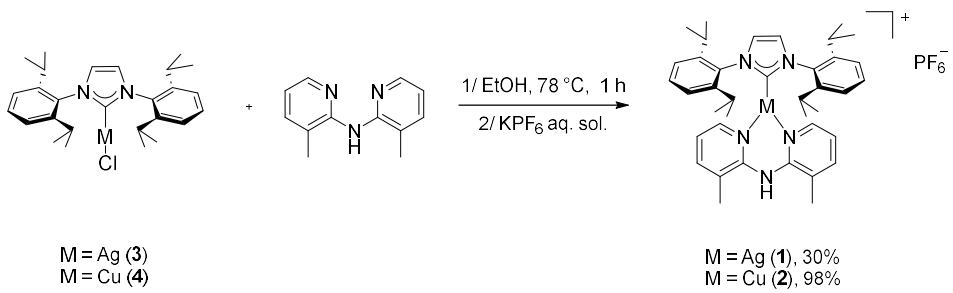

Scheme 1. Synthesis of **1** and **2**.

Table 1. Selected bond lengths (Å) and angles (°) from the X-ray diffraction analysis of **1** and **2**.

Complex	M – C_{IPr} [Å]	M – N [Å]	CH-C_g [Å]	N – M – N [°]	N – M – C_{IPr} [°]	Plane angle θ [°]
1	2.0744(15)	2.2872(14) 2.2889(14)	2.57 2.61	81.29(5)	138.19(6) 140.50(6)	18.29
2[a]	1.9208(18)	2.0577(18) 2.0590(17)	2.97 2.59	89.62(7)	135.94(7) 134.42(7)	22.40

[a] data previously reported in reference 33

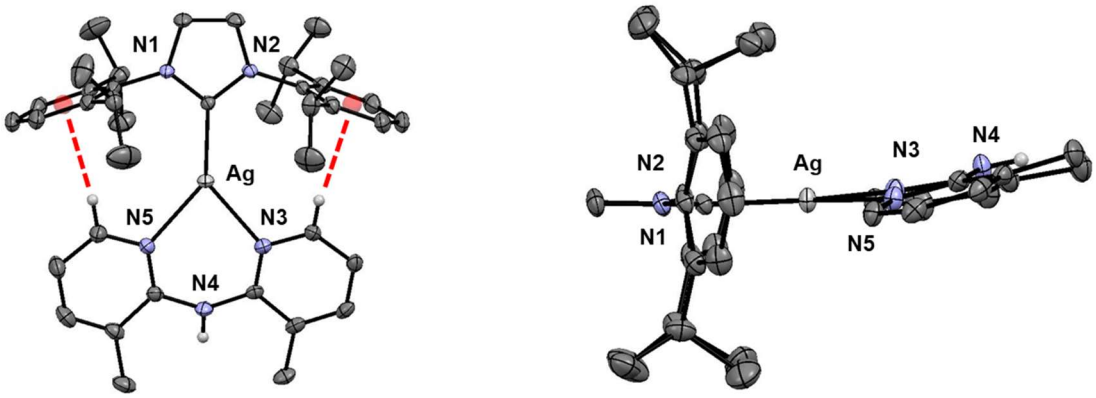

Figure 1. Ellipsoid representations at 50 % probability of the XRD analysis of **1** (side view on left and top view on right). Counterion and some hydrogen atoms were omitted for clarity.

Photophysical and computational studies

The absorption and emission spectra in solution and powder are shown in Figure 2, while the most relevant figures-of-merit for the emission are summarized in Table 2. The UV-visible absorption spectra of **1** and **2** were recorded in dichloromethane solution (10^{-5} M) (Figure 2, left). The absorption spectra showed bands in the far UV-region with maximum at 259 for **1** and 252 nm for **2**, respectively. According to time-dependent Density Functional Theory (TD-DFT) calculations, these features can be assigned to a $\pi - \pi^*$ ligand centered (LC) transitions for both the complexes. In addition, absorption features until 350 and 380 nm are also noted for **1** and **2**, respectively. According to analysis of Natural Transition Orbitals (NTOs), these lower energy bands displayed drastic different electronic transitions. In detail, **2** exhibited a broad band characterized by the excited states 4, 5 and 7 that are assigned to an admixture of LC in $^{3\text{-Me}}$dpa and MLCT from copper to $^{3\text{-Me}}$dpa (Figure S3 and Table S2 in ESI). In contrast, **1** showed two bands mainly driven by the first and third calculated excited states resulting from a ligand centered transitions (LC) located in $^{3\text{-Me}}$dpa (Figure S2 and Table S1 in ESI). In other words, the lowest singlet excited state of **1** present almost exclusively a LC transition with 97% on the transition being localized on the $^{3\text{-Me}}$dpa ligand, while **2** exhibit a pronounced MLCT character from the metal to $^{3\text{-Me}}$dpa ligand (69%) along some LC transition on the $^{3\text{-Me}}$dpa ligand (26%) (Figure 3).[19,33] Next, the emission features in solution and powder were studied. While they are not emissive in solution, the powder samples exhibit a strong, broad, and blue emission bands centered 3.07 eV (λ_{em} = 404 nm) and 2.72 eV (λ_{em} = 455 nm) for **1** and **2**, respectively (Figure 2, right). Theoretical calculations were in good agreement, predicting the $S_1 \rightarrow S_0$ transition at 2.77 eV (448 nm) for **1** and 2.43 eV (510 nm) for **2**. Please note that the difference on energy between the two set of data was resulting from the fact that the calculations were performed in vacuum. The blue-shifted emission between silver and its congener is not surprising since silver ion has bigger atomic radius compare to copper and the 4d orbitals of the silver metal center are lower energy level than copper.[23,40,41] As a consequence, the lowest lying excited state does not involve the metal center. Indeed, this was further confirmed by steady-state emission measurement at 77 K.

Table 2. Photophysical data of **1** and **2**.

Complex	λ_{abs}[a] [nm] (ε [10^4 L·mol^{-1}·cm^{-1}])	λ_{em}[b] [nm] 298 K	τ_{em}[b] 298 K	PLQY[b] [%]	λ_{em}[b] [nm] 77 K	τ_{em}[b] 77 K
1	259 [0.90] 288 (s) [0.65] 295 [0.71] 315 [0.70]	404[d]	7.4 ns[d]	25[d]	383[d]	9.5 ns[d]
2[c]	252 [0.44] 268 (s) [0.27] 302 [0.29] 318 (s) [0.23]	455[e]	44 µs[e]	86[e]	460[e]	81 µs[e]

[a] 10^{-5} in CH_2Cl_2 solution; [b] in powder; [c] data from reference 19; [d] λ_{ex} = 290 nm; [e] λ_{ex} = 365 nm.

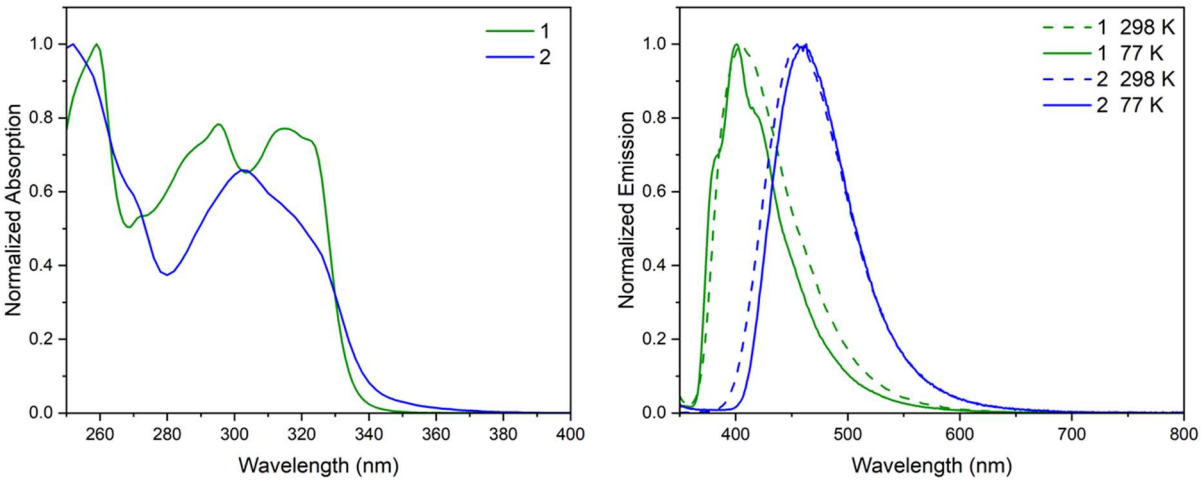

Figure 2. UV-visible spectra of **1** and **2** in dichloromethane solution (10^{-5} M), left; and emission spectra of **1** and **2** at 77 K (dash line) and 298 K (solid line), right.

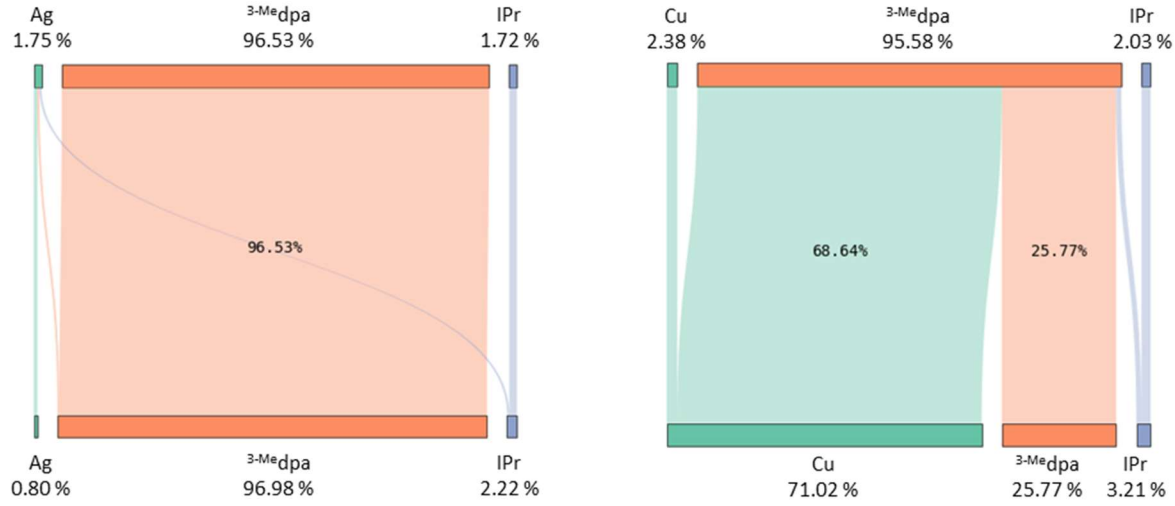

Figure 3. Transition diagram calculated on the Natural Transition orbital for the $S_0 \rightarrow S_1$ transition for the complexes [M(IPr)($^{3\text{-Me}}$dpa)][PF_6]. Left: complex **1** and, Right: complex **2**.

Here, the emission spectrum of **1** displayed the typical vibronic resolution of LC transitions (Figure 2, right). In contrast, the featureless emission band shape of **2** holds at 77 K, confirming the MLCT character of the excited state. More importantly, time-resolved spectroscopy assays showed that the lowest excited state of **1** should be correlated to a singlet excited state as the excited state lifetimes (τ) are *ca*. 7 and 9 ns at 298 and 77 K with a PLQY of 25 %, while **2** shows the typical TADF behavior with τ values of 44 (298 K) and 81 μs (77K) and PLQY of 86 %, (Table 2). This experimental observation was further confirmed by TD-DFT calculations showing a singlet-triplet energy splitting ($\Delta E_{S1\text{-}T1}$) of 0.32 eV for **1** when analog copper complex (**2**) featured a much smaller value of 0.14 eV (Figure S6). Of note, the fluorescence of **1** is in stark contrast with the dual phosphorescence emission of our previous silver complex exhibiting AIE.[32]

To evaluate the possibility of application in LECs, the photophysical properties of **1** in thin-film were studied. At first, the characterization of pristine thin film (15 mg/ml of **1** in ACN solution) spin-coated onto quartz slides was performed. Atomic Force Microscopy (AFM) inspection of the thin-films confirmed a smooth and homogenous morphology with root mean square roughness (RMS) of < 1 nm (Figure 4), indicating that they are adequate for device fabrication.

Compared to the emission features of **1** in powder, the pristine thin-film featured a broad red-shifted band (447 nm) associated to a dramatic decrease of the PLQY and τ (Table 3 and Figure 4). This is typically attributed to short-range aggregation occurring in thin-film, resulting in new non-radiative deactivation pathways related to film morphology (phase boundaries).[42] In contrast to similar trigonal silver(I) complexes,[32] the fluorescence nature of the emission holds with short τ values of 3 ns. To recover the emission features in thin-film, a 1% w/w of **1** was dispersed in poly(methyl methacrylate) (PMMA) matrix. This film featured a similar film morphology (Figure 4), but a broad emission band centered at 398 nm associated to a PLQY of 7 % and τ values of 1.3 ns (Table 2 and 3, and Figure S9). The poor recovery of the PLQY compared to that of powder samples (25 %, Table 2) is very surprisingly compared to the standard literature. First, pristine **2**-based films already showed a < 10 % loss in PLQY compared to powder samples.[20] Second, the dispersion of iTMCs in PMMA traditionally leads to highly

emissive films that are not suitable for thin-film lighting applications as the PMMA is a dielectric system, while the increase of the complex amounts gradually reduces the PLQY.[41] To fully investigate this behavior, we prepared PMMA films with a gradual increase in concentration of **1** i.e. 30, 70 and 90 % w/w.

As expected, the thin-films showed a poor morphology in which phase separation of aggregates of **1** and PMMA are clearly noted by AFM and detected by powder-XRD (Figure 4 and 5).

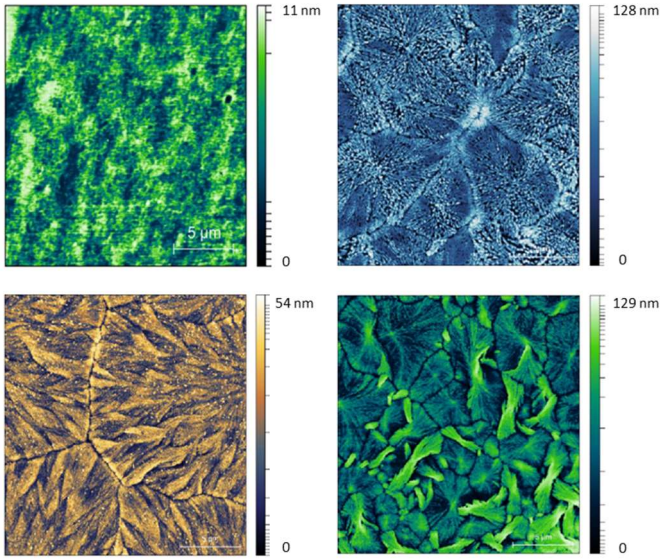

Figure 4. AFM pictures of thin films containing 1 % (top; left), 30 % (top; right), 70 % (bottom; left) and 90 % w/w (bottom; right) of **1** in PMMA.

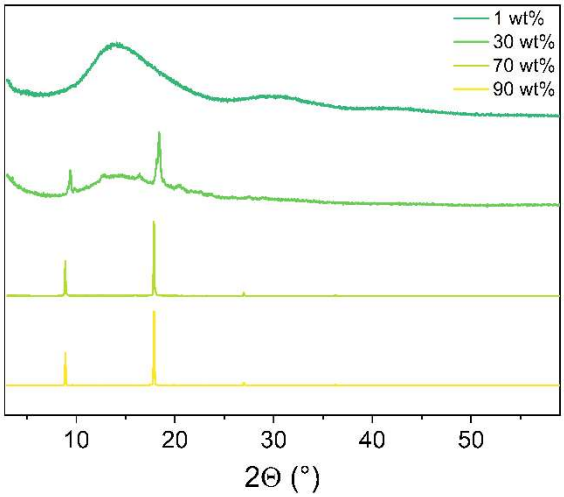

Figure 5. Powder-XRD of the thin films prepared with **1**.

Table 3. Photophysical data of **1** in thin-film.

Sample	λ_{em}[a] [nm]	τ_{em}[a] [ns]	PLQY[a] [%]
1 in pristine	447	3.0	2
1 % **1** in PMMA	398	1.3	7
30 % **1** in PMMA	407	2.7	12
70 % **1** in PMMA	402	5.3	18
90 % **1** in PMMA	400	5.4	23

[a] λ_{ex} = 290 nm

Thus, emissive films required a close rearrangement and/or packing of **1**. However, this film morphology is not suitable for thin-film lighting applications. A similar behavior has been recently shown in other trigonal silver (I) complexes in which AIE led to an efficient phosphorescent behavior that is lost in smooth and homogenous films applied in lighting devices.[32]

Electrochemical study in LEC devices

As a preliminary step towards implementing **1** in devices, cyclic voltammetry (CV) experiments were conducted in a THF solution (see Supporting Information). The resulting CV displayed broad features: i) two peaks in the cathodic scan at -1.55 V and -1.92 V, and ii) two peaks in the anodic scan at +0.77 V and +1.18 V. Interestingly, no sharp signal, assigned to the Ag(0) nanoclusters,[27,28] in the CV was observed at 0 V. Conseuently, we assumed that **1** was a potential candidate for LEC application as it appeared more stable than previous studied silver(I) complexes. Then, pristine **1**-based devices were prepared in spite of the their poor photophysical properties to study its electrical and electroluminescence behaviors. In short, LECs with a stacked two-layers architecture (ITO/PEDOT:PSS/**1**/Al) were prepared: a first layer (70 nm) of poly(3,4-ethylenedioxythiophene): polystyrene sulfonate (PEDOT:PSS) was spin-coated onto a clean indium-tin-oxide (ITO) electrode-coated glass; a layer of **1** was then prepared vis spin-coating from a 15 mg/ml acetonitrile solution, reaching a thickness of the film of 90 nm and a roughness below 1 nm (Figure 7, left); a final 100 nm layer of aluminum was prepared by physical vapor deposition. These devices were tested using a pulsed current of 8 mA with a 1 kHz block-wave and a 50 % duty cycle on 10 mm^2 pixels.

As expected from the low PLQY (Table 3) and the electron-hole recombination spin-statistic (25 % to singlets), **1**-based LEC did not show any luminance response. However, the electrical stability was remarkable with > 100 h (Figure 7, middle) stable voltage plateau after the exponential decay related to the formation of electrical double layers (EDL) at the electrode interface.[31,43,44] As reference, LECs with **2** showed a very poor electrochemical stability with a rise of the voltage over the first minutes.[20] This is a relevant result related to the state-of-the-art of silver(I) complexes in LECs.[27-28,30] Indeed, as mentioned above, the use of silver-based iTMC in LECs tend to form Ag(0) nanoclusters into the active layer that affect the properties of the device.[27,28] In detail, this causes, as first evidence, a linear and fast decrease of the average voltage due to the resistance drop inside the device.[28] As a second evidence, electrochemical impedance spectroscopy allows to monitor the changes in the device resistance (R_{LEC}) *vs*. the applied voltage associated to the formation of the EDLs and the electrochemical doping growth at lower and higher voltages. In the case of Ag(0) nanocluster formation, a sharp drop in R_{LEC} is noted.[28] In **1**-based LECs, the R_{LEC} profile of fresh and used devices is very similar with no indication of a severe electrochemical degradation. Finally, the stable electrical behavior allows to determine the dielectric constant (ε_r = 4.20) and ion conductivities ($\sigma = 1.04^{-7}$ S m^{-1}) obtained at 0 V (see experimental section) of the active layer. In

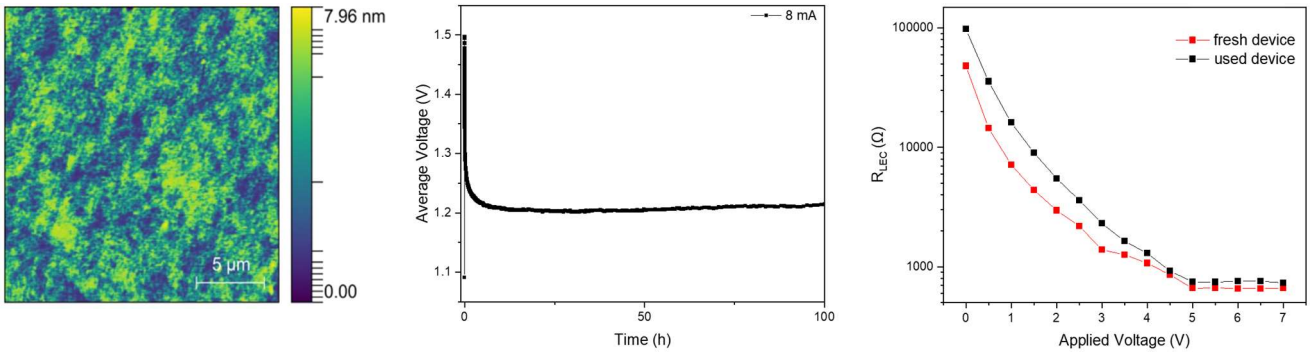

Figure 7. **1**-based LEC: AFM picture of the active layer (left), average voltage profile *vs* time (middle) and device resistance (R_{LEC}) *vs* applied potential (right).

line with the long time to reach the average voltage plateau compared to analogous LECs based on copper(I) and silver(I) complexes (i.e., few minutes vs. 5 h),[32] ε_r values are low compared to LECs. Of note, the dielectric constant was measured as ε_r = 13.95 for the recently reported [Ag(IPr)(bpy)][PF_6] complex,[32] indicating that the modification of the N^N ligand is an effective approach to modulate the rate of EDLs formation. In contrast, the ionic conductivity increased of one order of magnitude compared to [Ag(IPr)(bpy)][PF_6], suggesting an easier formation of the doped regions.[32]

Conclusions

In this work, we described the synthesis of the first cationic trigonal silver complex bearing NHC and dipyridylamine derivative as ligands and coordinated to the same combination of ligands than the best emitting previously reported copper(I) complex design applied in blue-emitting LECs. The silver(I) complex was structurally and photophysically characterized in comparison with its copper(I) analog. The change of the metal ion exerts a profound modification on the electronic configuration of the emitting excited state that is mainly driven by a fluorescence process from a ^{1}LC excited state, whereas the copper(I) complex emission corresponds to a TADF emission due to the strong MLCT character. What is more, the silver(I) complex shows an unexpected emission dependent to the crystallinity of the sample that significantly contrasts with similar copper(I) and silver(I) complexes. Unfortunately, this leads to non-emissive homogenous films that should be suitable for thin-film lighting applications. Thus, LECs based on the silver (I) complexes did not show any electroluminescence response, but a very stable electrical behavior over 100 h, as confirmed by stability assays and EIS. This suggests an extraordinary electrochemical stability of this family of complexes that significantly contrasts with those of copper(I) complexes (a few minutes stable) and other silver (I) complexes LECs that have featured electrical stabilities spanning from a few minutes to seconds, respectively. Thus, the electrical behavior of trigonal silver(I) complexes points out to open a new horizon for future LEC development with more sustainable emitters.

Experimental part

Synthesis. Commercially available compounds were used without additional purification. All the reactions were carried out using standard Schlenk technique under Ar atmosphere. Purchased solvents were degassed by Ar bubbling before the use. The details about the synthesis of [Cu(IPr)($^{3\text{-Me}}$dpa)][PF_6] was reported previously[33] and for [Ag(IPr)($^{3\text{-Me}}$dpa)][PF_6] were provided in the Supplementary Information.

Crystallography. Data sets were acquired from single-crystal samples employing a Brüker Kappa APEXII CCD diffractometer. Initial unit cell parameters were determined by fitting the angular settings of strong reflections collected during a 6.0° scan in 12 frames distributed over three distinct sections of the reciprocal space (36 frames in total). Cell refinement and data reduction were conducted using SAINT (Brüker AXS). Absorption correction was implemented through the multiscan method with SADABS 2012/1 (Brüker AXS). The structure was solved using direct methods and refined utilizing SHELXL-97 or SHELXL-2013 (Sheldrick). All non-hydrogen atoms underwent refinement using full-matrix least-squares with anisotropic displacement parameters, while hydrogen atoms were positioned in idealized positions. Short interactions were computed using Platon version 250 420. P-XRD measurements were performed on a Miniflex diffractometer (Rigaku, Tokyo, Japan) with a copper source (1.54 Å) and a silicon strip detector (D/teX Ultra, Rigaku), a goniometer radius of 150 mm; both Soller slits at 2.5°; a divergence slit fixed at 0.625°; an anti-scatter slit of 8 mm; and a kβ filter of 0.06 mm nickel foil. The powder was placed on a low background silicon wafer sample holder (cut 911). The samples used for P-XRD measurements were prepared via drop casting from an acetonitrile solution with complex x (1, 30, 70 and 90 wt%) and PMMA.

Photophysical measurements. UV–vis absorption spectra were obtained at room temperature from 10^{-5} M solutions in CH_2Cl_2

using a PerkinElmer Lambda 40 UV-visible spectrometer. Wavelengths are presented in nanometers (nm). Steady-state emission spectra and emission photoluminescence quantum yield (PLQY) were recorded using an FS5 Spectrofluorometer from Edinburgh Instruments. For the lifetime measurements Time-Correlated Single-Photo Counting (TCSPC) detectors were employed, along with picosecond pulsed diode lasers (EPL Series) and LEDs (EPLED Series) for excitation. Temperature-dependent measurements were conducted using an optical cryostat (SC-80 holder) with the FS5 Spectrofluorometer. In cases of biexponential decays of the excited state, intensity-weighted lifetime analysis was applied.[45]

Computational details. Geometries were optimized with the PBE0 functional and the effective core potential SDD was used for the copper atom while 6–31+G(d,p) basis set was used for remaining atoms. Additionally, DFT-D3 dispersion correction[46,47] was included for a better description of long-range interactions such as CH–π interactions, respectively between the dpa and NHC ligands. TD-DFT calculations were performed with the PBE0 functional, which has been shown to be particularly relevant to describe TADF events.[48] S_1 geometries were optimized by using the implemented TD-DFT gradients whereas T_1 geometries were obtained from open-spin-relaxed open shell calculations. Characterization of the nature of the S_0->S_1 transition were performed using the VALET python library[48] for Visual Analysis of Electronic Transitions.[49]

Device preparation and characterization. Indium–tin oxide (ITO) substrates, 130 nm in thickness, were purchased from Naranjo Substrates. The substrates underwent a cleaning process involving water-diluted Derquim detergent, distilled water, ethanol, and propan-2-ol, with each step performed in a warm ultrasonic bath. Following this, the substrates were dried with a nitrogen flow and treated in a UV-ozone cleaner. An aqueous solution of PEDOT:PSS (CleviosP VP.AI4083) was sonicated and diluted with propan-2-ol before spin-coating onto the substrates. Film preparation involved spin-coating and drying, with the resulting layers confirmed for suitable morphology using AFM. An aluminum cathode (100 nm) was deposited onto the active layer by physical vapor deposition. The device performance, including voltage and current profiles, was assessed using the Botest OLT OLED Lifetime-Test System in pulsed mode, with ITO serving as the anode and aluminum as the cathode. Time-dependent luminance and electroluminescence spectra were recorded using an Avantes spectrophotometer equipped with a calibrated integrating sphere. Electrochemical Impedance Spectroscopy (EIS) assays were carried out using a Metrohm Autolab III potentiostat/galvanostat with a frequency analyser module (FRA2) in the voltage range of 0 to 7 V, fitted with an equivalent circuit model described in Supporting information.

Conflicts of interest

There are no conflicts to declare.

Acknowledgements

This work was supported by the “Ministère de L’Ensignament Supérieur et de la Reserche”, CNRS (Centre National de la Recherche Scientifique) and LABEX SynOrg (ANR-11-LABX-0029). S.G. aknowledges the “Région Normandie” (G.G.), the Graduate School of Research XL-Chem (ANR-18-EURE-0020 XL-Chem) for funding.

References

1 R. D. Costa, Ed., Light-Emitting Electrochemical Cells, Springer International Publishing, Cham, 2017.
2 B. Meier, D. Tordera, A. Pertegás, C. Roldán-Carmona, E. Ortí and H. J. Bolink, *Materials Today*, 2014, **17**, 217–223.
3 H. Yersin, A. F. Rausch, R. Czerwieniec, T. Hofbeck, T. Fischer, *Coord. Chem. Rev.*, **255**, 21-22, 2622-2652
4 M. D. Weber, J. E. Wittmann, A. Burger, O. B. Malcıoğlu, J. Segarra-Martí, A. Hirsch, P. B. Coto, M. Bockstedte, R. D. Costa, *Adv. Funct. Mater.,* 2016, **37**, 6737-6750.
5 E. Fresta, G. Volpi, C. Garino, C. Barolo, R. D. Costa, *Polyhedron*, 2018, **140**, 129– 137
6 M. D. Weber, V. Nikolaou, J. E. Wittmann, A. Nikolaou, P. A. Angaridis, G. Charalambidis, C. Stangel, A. Kahnt, A. G. Coutsolelos, R. D. Costa, *Chem. Commun.*, 2016, **52**, 1602-1605.
7 E. Nannen, J. Frohleiks, S. Gellner, *Adv. Funct. Mater.,* 2020, **30**, 33, 1907349.
8 J. Frohleiks, S. Wepfer, Y. Kelestemur, H. V. Demir, G. Bacher, E. Nannen, *ACS Appl. Mater. Interfaces,* 2016, **8**, 37, 24692–24698
9 J. Gao, *ChemPlusChem*, 2018, **83**, 183–196.
10 5 D. Tordera, S. Meier, M. Lenes, R. D. Costa, E. Ortì, W. Safert, H. J. Bolink, *Adv. Mater.*, 2012, **24**, 897-900.
11 G. U. Mahoro, E. Fresta, M. Elie, D. di Nasso, Q. Zhang, J.-F. Lohier, J.-L. Renaud, M. Linares, R. Wannemacher, J. Cabanillas-Gonzalez, R. D. Costa and S. Gaillard, *Dalton Trans.*, 2021, **50**, 11049–11060.
12 E. Fresta, G. U. Mahoro, L. M. Cavinato, J.-F. Lohier, J.-L. Renaud, S. Gaillard and R. D. Costa, *Adv. Opt. Mat.*, 2022, **10**, 2101999.
13 G. U. Mahoro, J. Fernandez-Cestau, J.-L. Renaud, P. B. Coto, R. D. Costa and S. Gaillard, *Adv. Opt. Mat.*, 2020, **8**, 2000260.
14 C. E. Housecroft and E. C. Constable, *Coord. Chem. Rev.*, 2017, **350**, 155–177.
15 C. E. Housecroft and E. C. Constable, *J. Mater. Chem. C*, 2022, **10**, 4456–4482.
16 R. Czerwieniec, M. J. Leitl, H. H. H. Homeier and H. Yersin, *Coord. Chem. Rev.*, 2016, **325**, 2–28.
17 M. Alkan-Zambada, S. Keller, L. Martínez-Sarti, A. Prescimone, J. M. Junquera-Hernández, E. C. Constable, H. J. Bolink, M. Sessolo, E. Ortí and C. E. Housecroft, *J. Mater. Chem. C*, 2018, **6**, 8460-8471.
18 L. M. Cavinato, S. Wölfl, A. Pöthig, E. Fresta, C. Garino, J. Fernandez-Cestau, C. Barolo, R. D. Costa, *Advanced Mater.*, 2022, **34**, 12, 2109228
19 M. Elie, F. Sguerra, F. Di Meo, M. D. Weber, R. Marion, A. Grimault, J.-F. Lohier, A. Stallivieri, A. Brosseau, R. B. Pansu, J.-L. Renaud, M. Linares, M. Hamel, R. D. Costa and S. Gaillard, *ACS Appl. Mater. Interfaces*, 2016, **8**, 14678.
20 M. D. Weber, E. Fresta, M. Elie, M. E. Miehlich, J.-L. Renaud, K. Meyer, S. Gaillard and R. D. Costa, *Adv. Funct. Mater.*, 2018, **28**, 1707423.

21 A. Kaeser, O. Moudam, G. Accorsi, I. Séguy, J. Navarro, A. Belbakra, C. Duhayon, N. Armaroli, B. Delavaux-Nicot, J.-F. Nierengarten, *Eur. J. Inorg. Chem.*, 2014, **2014**, 1345–1355.

22 14 O. Moudam, A. Kaeser, B. Delavaux-Nicot, C. Duhayon, M. Holler, G. Accorsi, N. Armaroli, I. Séguy, J. Navarro, P. Destruel, J.-F. Nierengarten, *Chem. Commun.*, 2007, 3077–3079.

23 C.-W. Hsu, C.-C. Lin, M.-W. Chung, Y. Chi, G.-H. Lee, P.-T. Chou, C.-H. Chang and P.-Y. Chen, *J. Am. Chem. Soc.*, 2011, **133**, 12085–12099.

24 K. Matsumoto, T. Shindo, N. Mukasa, T. Tsukuda, T. Tsubomura, *Inorg. Chem.*, 2012, **51**, 5805–5813.

25 C.-C. Hsu, C.-C. Lin, P.-T. Chou, C.-H. Lai, C.-W. Hsu, C.-H. Lin, Y. Chi, *J. Am. Chem. Soc.*, 2012, **134**, 7715–7724.

26 H. Kunkely, A. Vogler, *Inorganica Chim. Acta*, 2006, **359**, 388–390.

27 O. Moudam, A. C. Tsipis, S. Kommanaboyina, P. N. Horton, S. J. Coles, *RSC Adv.*, 2015, **5**, 95047–95053.

28 E. Fresta, J. M. Carbonell-Vilar, J. Yu, D. Armentano, J. Cano, M. Viciano-Chumillas and R. D. Costa, *Adv. Funct. Mater.,* 2019, **29**, 1901797.

29 M. D. Weber, M. Viciano-Chumillas, D. Armentano, J. Cano and R. D. Costa, *Dalton Trans.*, 2017, **46**, 6312–6323.

30 S. Lipinski, L. M. Cavinato, T. Pickl, G. Biffi, A. Pöthig, P. B. Coto, J. Fernández-Cestau and R. D. Costa, *Adv. Opt. Mater.*, 2023, **11**, 2203145.

31 E. Fresta, M. D. Weber, J. Fernandez-Cestau and R. D. Costa, *Adv. Opt. Mater.*, 2019, **7**, 1900830.

32 G. Giobbio, P. B. Coto, J.-F. Lohier, J.-L. Renaud, S. Gaillard and R. D. Costa, *Dalton Trans.*, 2024, **53**, 12307-12315R.

33 Marion, F. Sguerra, F. Di Meo, E. Sauvageot, J.-F. Lohier, R. Daniellou, J.-L. Renaud, M. Linares, M. Hamel and S. Gaillard, *Inorg. Chem.*, 2014, **53**, 9181–9191.

34 M. Elie, M. D. Weber, F. Di Meo, F. Sguerra, J.-F. Lohier, R. B. Pansu, J.-L. Renaud, M. Hamel, M. Linares, R. D. Costa and S. Gaillard, *Chem. Eur. J.*, 2017, **23**, 16328–16337.

35 E. Sauvageot, R. Marion, F. Sguerra, A. Grimault, R. Daniellou, M. Hamel, S. Gaillard and J.-L. Renaud, *Org. Chem. Front.*, 2014, **1**, 639-644.

36 P. de Frémont, N. M. Scott, E. D. Stevens, T. Ramnial, O. C. Lightbody, C. L. B. Macdonald, J. A. C. Clyburne, C. D. Abernethy and S. P. Nolan, *Organometallics*, 2005, **24**, 6301–6309.

37 C. A. Citadelle, E. L. Nouy, F. Bisaro, A. M. Z. Slawin and C. S. J. Cazin, *Dalton Trans.,* 2010, **39**, 4489.

38 O. Santoro, A. Collado, A. M. Z. Slawin, S. P. Nolan and C. S. J. Cazin, *Chem. Commun.*, 2013, **49**, 10483.

39 E. Clementi, D. L. Raimondi and W. P. Reinhardt, *J. Chem. Phys.*, 1967, **47**, 1300–1307.

40 M. Z. Shafikov, A. F. Suleymanova, R. Czerwieniec and H. Yersin, *Chem. Mater.,* 2017, **29**, 1708–1715.

41 M. Z. Shafikov, R. Czerwieniec and H. Yersin, *Dalton Trans.*, 2019, **48**, 2802–2806.

42 J. Mei, N. L. C. Leung, R. T. K. Kwok, J. W. Y. Lam and B. Z. Tang, *Chem. Rev.*, 2015, **115**, 11718–11940.

43 B. M. D. Puscher, M. F. Aygüler, P. Docampo and R. D. Costa, *Adv. Energy Mater.*, 2017, **7**, 1602283.

44 M. D. Weber, M. Viciano-Chumillas, D. Armentano, J. Cano and R. D. Costa, *Dalton Trans.*, 2017, **46**, 6312–6323.

45 A. Sillen, Y. Engelborghs, *Photochem. Photobiol.*, 1998, **67**, 475.

46 S. Grimme, S. Ehrlich, L. Goerigk, *J. Comput. Chem.,* 2011, **32**, 1456–1465.

47 S. Grimme, J. Antony, S. Ehrlich, H. Krieg, *J. Chem. Phys.*, 2010, **132**, 154104.

48 M. Moral, L. Muccioli, W.-J. Son, Y. Olivier, J.-C. Sancho-García, *J. Chem. Theory Comput.*, 2015, **11**, 168–177.

49 https://github.com/tbmasood/VALET